# DATA-DRIVEN SAW-CUT IDENTIFICATION IN STEEL BEAMS USING ANN: ADDRESSING GENERALIZATION CHALLENGES IN UNSEEN AND OUT-OF-DISTRIBUTION SCENARIOS

NHẬN DẠNG VẾT CẮT CƯA DỰA TRÊN DỮ LIỆU TRÊN KẾT CẤU DẦM THÉP SỬ DỤNG MẠNG NƠ-RON NHÂN TẠO: GIẢI QUYẾT CÁC THÁCH THỨC VỀ KHẢ NĂNG TỔNG QUÁT HÓA TRONG CÁC KỊCH BẢN CHƯA BIẾT VÀ NGOÀI PHÂN PHỐI

**VAN TUAN VU**[a,*], **DUC TUAN TA**[a]
[a]Le Quy Don Technical University
*Corresponding author: *Email:* vantuanvu@lqdtu.edu.vn
*Article history: Received 15/4/2026, Revised 14/5/2026, Accepted 20/5/2026*
https://doi.org/10.59382/j-ibst.2026.vi.vol2-3

Abstract: *Ensuring the structural integrity of beam-like structures is vital for civil and mechanical engineering. However, reliable structural health monitoring (SHM) faces significant challenges due to the scarcity of real-world damage data and the difficulty of predicting damage parameters (width and depth) in unseen scenarios. This study proposes a robust hybrid framework that integrates the Finite Element Method (FEM), the Rational Fraction Polynomial (RFP) experimental method, and Artificial Neural Networks (ANN) to predict the characteristics of saw-cut damage in steel beams. A comprehensive dataset was generated via FEM and validated against experimental measurements to bridge the gap between simulation and reality. Two distinct ANN architectures were investigated: a data-driven optimized model (ANN_1) and a theory-based shallow network (ANN_2). Notably, the study reveals a dual contribution: while ANN_1 excels in multi-parameter characterization of location, width, and depth, the shallow ANN_2 model achieves comparable accuracy for location-only prediction ( $R^2$>0.97) at a fraction of the computational cost, thereby supporting a tiered deployment strategy for practical SHM applications. Furthermore, permutation importance analysis reveals that the first natural frequency (F1) is the dominant feature for location and width, whereas the second natural frequency (F2) is critical for depth estimation. Overall, the proposed approach provides an efficient and reliable solution for real-world SHM applications, particularly in scenarios where structural conditions are unpredictable.*

Keywords: *Structural Health Monitoring, Steel Beams, Finite Element Method, Artificial Neural Networks, Damage Characterization, Generalization Capability.*

Tóm tắt: *Việc đảm bảo tính toàn vẹn kết cấu của các cấu kiện dạng dầm là cực kỳ quan trọng trong kỹ thuật dân dụng và cơ khí. Tuy nhiên, công tác giám sát sức khỏe kết cấu (SHM) đang đối mặt với những thách thức lớn do sự khan hiếm dữ liệu hư hại thực tế và độ khó trong việc dự đoán các tham số hình học (chiều rộng và chiều sâu) trong các kịch bản chưa biết. Nghiên cứu này đề xuất một khung làm việc hỗn hợp mạnh mẽ, tích hợp phương pháp Phần tử hữu hạn (FEM), phương pháp thực nghiệm Rational Fraction Polynomial (RFP) và mạng thần kinh nhân tạo (ANN) để dự đoán đặc điểm vết cắt cưa trong dầm thép. Một bộ dữ liệu toàn diện đã được tạo ra thông qua FEM và được kiểm chứng bằng các phép đo thực nghiệm nhằm thu hẹp khoảng cách giữa mô phỏng và thực tế. Hai cấu trúc ANN khác nhau đã được nghiên cứu: mô hình tối ưu hóa dựa trên dữ liệu (ANN_1) và mạng nông dựa trên lý thuyết (ANN_2). Kết quả cho thấy mặc dù cả hai mô hình đều hoạt động đáng tin cậy trong việc xác định vị trí hư hại—trong đó mạng nông ANN_2 vẫn cung cấp độ chính xác đủ dùng cho nhiệm vụ cụ thể này—nhưng ANN_1 vượt trội hơn hẳn ANN_2 trong việc dự đoán các tham số hình học phức tạp (chiều rộng và chiều sâu). Đáng chú ý, nghiên cứu này cho thấy đóng góp kép: trong khi ANN_1 vượt trội trong việc mô tả đa tham số về vị trí, chiều rộng và chiều sâu, mô hình ANN_2 đơn giản hơn đạt được độ chính xác tương đương cho dự đoán chỉ vị trí ($R^2$>0,97) với chi phí tính toán thấp hơn nhiều, từ đó hỗ trợ chiến lược triển khai theo cấp bậc cho các ứng dụng SHM thực tế. Hơn nữa, phân tích tầm quan trọng của đặc trưng (permutation importance) cho thấy tần số dao động tự nhiên thứ nhất (F1) là đặc trưng chủ đạo để xác định vị trí và chiều rộng, trong khi tần số dao động tự nhiên thứ hai (F2) đóng vai trò then chốt trong việc ước tính chiều sâu. Phương pháp đề xuất cung cấp một giải pháp hiệu quả và đáng tin cậy cho các ứng dụng SHM thực tế, đặc biệt là trong các kịch bản mà điều kiện kết cấu không thể dự đoán trước.*

Từ khóa: *Giám sát sức khỏe kết cấu, dầm thép, phương pháp phần tử hữu hạn, mạng thần kinh nhân tạo, đặc tính hóa hư hại, khả năng tổng quát hóa.*

## 1. Introduction

Beams are key structural members that are extensively employed in civil and mechanical engineering applications. The detection and evaluation of damage in beam-like structures are vital for maintaining safety and ensuring proper functionality. Over the years, numerous analytical and numerical techniques have been proposed for crack identification in beams. Early investigations by Yang, Swamidas [22] and Swamidas, Yang [19] utilized classical beam theories together with energy-based formulations to detect cracks in vibrating systems. Subsequently, vibration-based approaches have attracted considerable attention due to their non-destructive characteristics and their high sensitivity to structural modifications. Several studies, such as those by Gillich, Praisach [8], Zhou, Maia [24] Gillich, Furdui [7]  Zhou, Maia [23] and Vu[20, 21] demonstrated that variations in modal properties, particularly natural frequencies, can serve as effective indicators of structural damage.

In recent years, machine learning (ML) techniques have become increasingly prominent in structural health monitoring (SHM), offering data-driven solutions that eliminate the need for explicit physical modeling. Various ML methods have been applied to crack detection problems. For example, Samir, Idir [16] employed genetic algorithms to locate damage based on frequency variations, while Ghadimi and Kourehli [6] utilized modified extreme learning machines to accurately identify crack positions. Artificial Neural Networks (ANNs) are especially popular due to their ability to approximate complex nonlinear relationships. For instance, Lee, Kim [12] applied ANN models for crack detection in pipelines, whereas Mortazavi and Ince [13] developed ANN-based approaches for predicting fatigue crack growth. More recent works have combined ANN with modal analysis and numerical simulations to improve predictive capability, as reported by Gillich, Tufisi [9], Seguini, Djamel [17]. In addition, hybrid techniques that integrate optimization algorithms with machine learning models, such as those presented in [18] and Cuong-Le, Nghia-Nguyen [5] have shown enhanced performance in complex damage identification scenarios.

Despite these advancements, a significant challenge in ML-based damage detection is the limited availability of reliable training data. In practical applications, monitoring data typically correspond to normal operating conditions or minor damage cases, whereas severe damage scenarios are rarely recorded. This imbalance makes it difficult to construct comprehensive datasets for training robust ML models. Moreover, important fracture-related parameters, such as stress intensity factors and crack propagation characteristics, are often difficult to be measured directly in real structures.

To overcome this limitation, numerical modeling approaches—especially the Finite Element Method (FEM)—have been extensively employed to produce synthetic datasets that capture a wide range of damage conditions. It has been demonstrated from previous research works that FEM is capable of accurately representing structural responses and supplying dependable input data for machine learning applications (Khatir and Wahab [11] and Khatir, Khatir [10]). Furthermore, when integrated with experimental identification techniques such as the Rational Fraction Polynomial (RFP) method, FEM-based models can be systematically validated and calibrated, thereby enhancing their predictive accuracy.

In the present study, the term "damage" specifically refers to saw-cut (notch-like) damage represented by localized stiffness and mass reduction in steel beams, and does not include other structural failure mechanisms such as local or global buckling. Although substantial advancements have been achieved in vibration-based damage detection and the application of machine learning techniques, several important challenges remain unresolved. To begin with, many studies depend largely on datasets generated either from numerical simulations alone or from a limited number of experimental observations, which may not adequately capture the full variability and complexity encountered in real structures. In addition, model performance is often assessed using datasets where training and testing samples follow similar statistical distributions, making it difficult to evaluate true generalization capability. Notably, the ability of models to identify damage at entirely new and previously unobserved locations—an essential requirement for practical structural health monitoring—remains insufficiently explored. This limitation can be addressed by constructing more rigorous evaluation strategies; for example, reserving a subset of data that includes unseen damage locations and extrapolation cases—such as 40 testing scenarios, including entirely new locations and 10 cases with width and depth values exceeding the training range—provides a more realistic assessment of model performance. Moreover, while theoretical work has established the approximation power of shallow neural networks, there is a lack of comprehensive comparisons between theory-guided model configurations and data-driven optimization strategies in complex engineering contexts. These gaps underscore the necessity of developing an integrated framework that incorporates validated numerical modeling, experimental validation, and rigorous testing on unseen scenarios to ensure both accuracy and robustness in damage prediction.

Building on the considerations outlined above, this study offers several key contributions to the field of structural health monitoring. First, it proposes a hybrid framework that combines experimental modal analysis using the Rational Fraction Polynomial (RFP) method, numerical modeling via the Finite Element Method (FEM), and Artificial Neural Networks (ANN) to achieve robust damage identification in beam structures. Second, a comprehensive dataset is constructed through FEM simulations and subsequently validated with experimental measurements, thereby mitigating the challenge of limited real-world data availability. Third, two ANN architectures with distinct design philosophies are systematically examined, namely a data-driven optimized model (ANN_1) and a theory-guided shallow network (ANN_2), enabling a comparative assessment of different model development strategies. Finally, the proposed framework is rigorously tested on a dataset composed entirely of previously unseen damage locations, demonstrating the strong generalization performance and practical relevance of the optimized ANN model.

## 2. Natural frequencies are obtained by employing both the Rational Fraction Polynomial (RFP) approach and Finite Element Method (FEM) simulations

### *2.1 Estimation of natural frequencies in steel beams using the Rational Fraction Polynomial (RFP) method*

The experimental study was carried out on steel cantilever beams with rectangular coss-section with geometric dimensions of 1005 mm in length, 42 mm in width, and 10 mm in height. The material characteristics of the beams include a Young's modulus of 200 GPa and a mass density of 7850 kg/m³ (see Table 1).

**Table 1.** *Geometric and material characteristics of the steel beam*

| No. | Parameter | Unit | Value |
|---|---|---|---|
| 1 | Structural length | mm | 1005 |
| 2 | Cross-sectional height | mm | 10 |
| 3 | Cross-sectional width | mm | 42 |
| 4 | Mass density | kg/m³ | 7850 |
| 5 | Modulus of elasticity | GPa | 200 |

A localized defect was introduced by machining a notch with dimensions of 2 mm in width and 5 mm in depth, positioned 220 mm from the fixed support, as shown in Figure 1. The natural frequencies of the beam, in both intact and damaged states, were determined through impact-based modal testing. Five PCB piezoelectric accelerometers were used to record the dynamic response signals, with their added mass considered negligible. Data acquisition and processing were conducted using B&K Connect™ software, while modal parameters were identified through the Rational Fraction Polynomial (RFP) method implemented within the software. The extracted natural frequencies are summarized in Table 2.

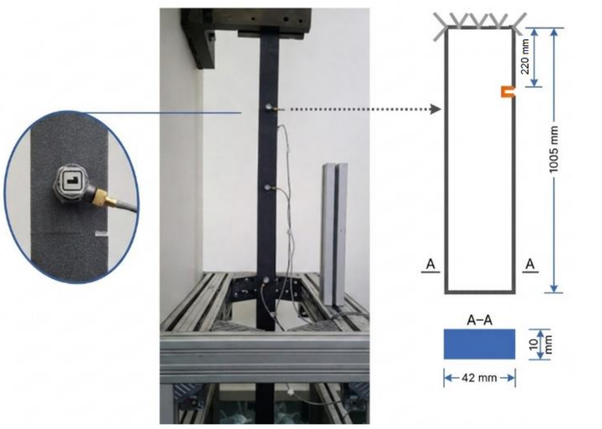


**Figure 1.** *Laboratory setup for experimental testing of the cantilever beam*

**Table 2.** *Natural frequencies of the cantilever beam determined through experimental measurements*

| No. | Damage location | | Natural frequency (Hz) | | | |
|---|---|---|---|---|---|---|
| | x0 (mm) | d (mm) | Mode 1 | Mode 2 | Mode 3 | Mode 4 |
| Undamaged | - | - | 7.769 | 48.366 | 137.350 | 277.269 |
| Damaged | 220 | 5 | 7.767 | 48.365 | 137.339 | 277.240 |

### *2.2 Finite Element Method (FEM)–based analysis for identifying the natural frequencies of a steel beam*

While the Finite Element Method (FEM) is widely utilized for modeling cracks, reproducing realistic crack conditions in laboratory experiments remains challenging. In practice, some studies approximate cracks in beam specimens by using saw-cut notches [17, 18], however, such approaches do not fully replicate the behavior of actual cracks. In contrast to saw-cuts, real cracks primarily modify the cross-sectional stiffness of the beam without significantly altering its mass, and their geometry is often difficult to characterize precisely. Consequently, to ensure better consistency between numerical simulations and experimental observations, this study employs saw-cuts as a practical representation of beam damage within the FEM framework.

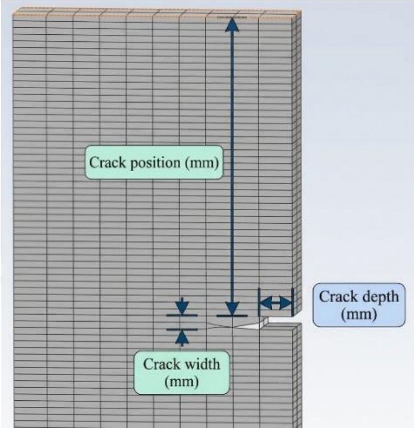


**Figure 2.** *FEM-based modeling of the beam structure including a saw-cut damage feature*

**Table 3.** *Intrinsic material and physical parameters of the undamaged structure*

| No. | Natural frequencies determined via the Rational Fraction Polynomial (RFP) technique (Hz) | Finite element method (Hz) | Error (%) |
|---|---|---|---|
| 1 | 7.769 | 7.780 | 0.15 |
| 2 | 48.366 | 48.737 | 0.77 |
| 3 | 137.35 | 136.378 | 0.71 |

**Table 4.** *Physical Properties of the damaged structure*

| No. | Natural frequencies determined via the Rational Fraction Polynomial (RFP) technique (Hz) | Finite element method (Hz) | Error (%) |
|---|---|---|---|
| 1 | 7.767 | 7.767 | 0.00 |
| 2 | 48.365 | 48.739 | 0.77 |
| 3 | 137.339 | 136.295 | 0.76 |

A finite element model was constructed in Ansys using three-dimensional elastic beam elements, as illustrated in Figure 2. The mesh was carefully refined to enable accurate representation of the saw-cut defect and to closely match the experimentally measured natural frequencies. It was found that discretizing the beam into 20,100 elements yielded the most accurate results. The numerical predictions exhibited strong agreement with the experimental data for both intact and damaged conditions, as summarized in Table 3 and Table 4. In this experiment, the oscillation parameters were determined using the Rational Fraction Polynomial (RFP) method integrated into the software. The RFP method is primarily used in the step of identifying modal parameters from FRF (Frequency Response Function) data, then monitoring changes in natural frequencies, damping ratios, and mode shapes to infer the likelihood of structural damage or stiffness degradation. Essentially, it's a frequency-domain curve fitting technique, approximating the measured FRF using a rational function whose numerator and denominator are polynomials in the frequency/complex variable. The poles of the denominator provide modal information, while residue/modal constants relate to the mode shape[14].

**Table 5.** *Database developed using Finite Element Analysis (FEA)*

| No. | Damage Location (mm) | Crack Width (mm) | Crack Depth (mm) | Natural frequencies | | |
|---|---|---|---|---|---|---|
| | | | | Mode 1 (Hz) | Mode 2 (Hz) | Mode 3 (Hz) |
| 1 | 10 | 2 | 5 | 7.749 | 48.221 | 137.000 |
| 2 | 20 | 2 | 5 | 7.748 | 48.226 | 137.037 |
| 3 | 30 | 2 | 5 | 7.749 | 48.240 | 137.095 |
| 4 | 40 | 2 | 5 | 7.750 | 48.253 | 137.150 |
| 5 | 50 | 2 | 5 | 7.751 | 48.266 | 137.198 |
| … | … | … | … | … | … | … |
| 22 | 220 | 2 | 5 | 7.767 | 48.365 | 137.339 |
| 23 | 230 | 2 | 5 | 7.762 | 48.368 | 137.281 |
| 24 | 240 | 2 | 5 | 7.762 | 48.368 | 137.266 |
| 25 | 250 | 2 | 5 | 7.763 | 48.367 | 137.252 |
| 26 | 260 | 2 | 5 | 7.763 | 48.365 | 137.239 |

| No. | Damage Location (mm) | Crack Width (mm) | Crack Depth (mm) | Natural frequencies | | |
|---|---|---|---|---|---|---|
| | | | | Mode 1 (Hz) | Mode 2 (Hz) | Mode 3 (Hz) |
| … | … | … | … | … | … | … |
| 294 | 960 | 4 | 5 | 7.781 | 48.395 | 137.437 |
| 295 | 970 | 4 | 5 | 7.781 | 48.399 | 137.452 |
| 296 | 980 | 4 | 5 | 7.782 | 48.402 | 137.468 |
| 297 | 990 | 4 | 5 | 7.782 | 48.406 | 137.486 |
| 298 | 0 | 0 | 0 | 7.769 | 48.366 | 137.350 |
| … | … | … | … | … | … | … |
| 434 | 514 | 2 | 13 | 7.761 | 47.953 | 137.350 |
| 435 | 614 | 2 | 13 | 7.770 | 47.996 | 136.632 |
| 436 | 714 | 2 | 13 | 7.776 | 48.150 | 136.061 |
| 437 | 814 | 2 | 13 | 7.779 | 48.299 | 136.594 |
| 438 | 914 | 2 | 13 | 7.782 | 48.380 | 137.301 |

**Table 6.** *Distribution and bounds of variables in the training dataset*

| No. | Variable | unit | count | max | min |
|---|---|---|---|---|---|
| 1 | Location | mm | 398 | 995 | 0 |
| 2 | width | mm | 398 | 4 | 0 |
| 3 | depth | mm | 398 | 9 | 0 |
| 4 | Mode 1 | Hz | 398 | 7.782 | 7.706 |
| 5 | Mode 2 | Hz | 398 | 48.406 | 47.999 |
| 6 | Mode 3 | Hz | 398 | 137.486 | 136.424 |

To represent beam damage, the elements associated with the saw-cut region were removed from the model (Figure 2). In total, 438 damage cases were generated, of which 398 cases (No. 1–398) were used for training the machine learning models. The remaining 40 cases were reserved for testing, including scenarios with entirely new damage locations and 10 cases featuring width and depth values beyond the range of the training dataset (Table 7). The training dataset was initially produced using the FEM approach, while machine learning models were subsequently employed to predict damage characteristics based on natural frequencies obtained via the RFP method. Due to systematic differences between the frequencies computed by FEM and those identified through RFP, the FEM results were corrected using the average deviation observed in both intact and damaged conditions. The adjusted natural frequencies for each damage scenario are summarized in Table 5.

Although the dataset comprising 398 training samples and 40 testing samples may appear modest by deep learning standards, it is well-suited to the present low-dimensional regression problem, which involves only three input features ($F_1$, $F_2$, $F_3$) mapped to three output targets. The resulting sample-to-feature ratio (≈ 133:1) substantially exceeds conventional thresholds for regression modeling. Furthermore, since the dataset is generated through a validated FEM model, it is free from measurement noise, enabling the ANN to learn the underlying physical relationships efficiently. The test set was intentionally designed to include unseen spatial locations and 10 out-of-distribution cases with width and depth values exceeding the training range, thereby providing a rigorous evaluation of model extrapolation rather than a routine interpolation test. Table 6 summarizes the ranges of variables within the dataset, which play a critical role in the prediction process as they establish the operational limits of the model.

**Table 7.** *Distribution and bounds of variables in the testing dataset*

| No. | Variable | unit | count | max | min |
|---|---|---|---|---|---|
| 1 | Location | mm | 40 | 995 | 0 |
| 2 | width | mm | 40 | 6 | 0 |
| 3 | depth | mm | 40 | 13 | 0 |
| 4 | Mode 1 | Hz | 40 | 7.782 | 7.706 |
| 5 | Mode 2 | Hz | 40 | 48.406 | 47.953 |
| 6 | Mode 3 | Hz | 40 | 137.486 | 136.061 |

## 3. Construction of the artificial neural network (ANN) model

The machine learning models developed in this study were implemented in Python (version 3.11.0) using the Scikit-learn library. The input features consisted of natural frequencies corresponding to three vibration modes, while the predicted outputs represented the geometric parameters of the saw-cut, including its location, width, and depth.

### *3.1 Data preprocessing and partitioning for the development of the model*

The dataset was divided into training and testing subsets for the purposes of model development and performance evaluation. Before training, all input and output variables were normalized to the range [0, 1] to ensure uniform scaling and balanced influence during the learning process. The normalization applied to each variable is expressed as:

$$x_n = \frac{x - x_{\min}}{x_{\max} - x_{\min}} \tag{1}$$

where $x_{max}$ and $x_{min}$ denote the maximum and minimum values of each variable x, respectively.

### *3.2 Evaluation of the predictive performance and accuracy of the model*

The selection of suitable evaluation metrics is critical for assessing machine learning models, particularly in regression tasks. Among the most commonly used indicators are the coefficient of determination ($R^2$) and the mean squared error (MSE). The $R^2$ metric, which ranges from 0 to 1, quantifies the proportion of variance in the target variable that is captured by the model, with higher values reflecting stronger explanatory capability. However, it can sometimes yield overly optimistic interpretations in the case of highly complex models. In contrast, MSE measures the average of the squared differences between predicted and actual values, where lower values indicate better predictive accuracy and a greater sensitivity to large errors. Considering both $R^2$ and MSE together provides a more comprehensive and balanced evaluation of model performance.

$$R_{squared} = 1 - \frac{\sum_{i=1}^{n}\left(Y_i - y_i\right)^2}{\sum_{i=1}^{n}\left(Y_i - \bar{Y}\right)^2} \tag{2}$$

$$MSE = \frac{1}{n}\sum_{i=1}^{n}\left(Y_i - y_i\right)^2 \tag{3}$$

In this formulation, $Y_i$ represents the observed values, $y_i$ denotes the predicted outputs, and $\bar{Y}$ represents the average of the observed dataset.

### *3.3 Artificial Neural Network Models*

Artificial neural networks (ANNs) are data-driven computational frameworks inspired by the architecture and operation of the human brain. Like traditional statistical methods, they aim to model the relationship between input and output variables. However, instead of relying on predefined equations, ANNs learn these relationships directly from data. This enables them to effectively represent complex nonlinear behaviors and uncover underlying patterns, leading to enhanced predictive capability.

In this study, a multilayer feedforward neural network was employed and trained using the backpropagation algorithm, as introduced by Rumelhart, Hinton [15]. The network consists of interconnected computational units, known as neurons, which are connected via weighted links. These neurons are arranged in a series of layers, including an input layer, one or more hidden layers, and an output layer. This layered architecture facilitates effective information flow from inputs to outputs and strengthens the model's ability to learn complex patterns within the data.

The overall structure and functioning principles of artificial neural networks (ANNs) are well established in the literature. As depicted in Figure 3 (adapted from Shahin [4]), each neuron receives input signals ($\boldsymbol{x_i}$) from the previous layer, which are scaled by corresponding connection weights ($\boldsymbol{w_{ji}}$) and then summed. A bias term ($\boldsymbol{\theta_j}$) is added to this weighted sum ($\boldsymbol{I_j}$). The resulting value is subsequently processed through a nonlinear activation function $\boldsymbol{f}(\cdot)$, , typically a sigmoid or hyperbolic tangent function. This transformation produces the output ($\boldsymbol{y_j}$) allowing the network to capture complex and nonlinear relationships between inputs and outputs.

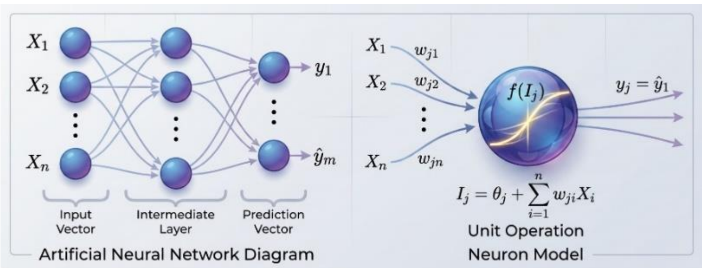


**Figure 3.** *Architecture and computational principles of artificial neural networks (AI-generated illustration)*

The training of the multilayer feedforward network starts with the initialization of model parameters, as illustrated in Figure 3. A learning algorithm is then employed to produce the network outputs, followed by iterative adjustments of the weights and biases to reduce the difference between predicted and target values. This optimization procedure continues until a specified convergence condition or acceptable error level is reached. After the training phase, the model is validated using an independent test dataset to evaluate its generalization performance. A detailed overview of ANN development procedures is provided by Maier and Dandy [3].

The choice of network architecture and hyperparameter configuration plays a critical role in ensuring robust model performance. Important considerations include the number of hidden layers and neurons, which govern the model's ability to capture complex patterns, and the learning rate, which affects both convergence behavior and training stability. A proper balance among these factors is necessary to prevent underfitting or overfitting. Furthermore, the number of training epochs should be selected carefully to allow adequate learning while preserving generalization capability. In the absence of universal design rules, the optimal setup is typically determined through systematic experimentation and comparative evaluation across different network configurations.

To evaluate the predictive performance of artificial neural networks for the problem under consideration, two ANN models with differing levels of complexity were developed and compared. The first model (ANN_1) was configured using a data-driven hyperparameter optimization strategy to maximize predictive accuracy and generalization capability. In contrast, the second model (ANN_2) was designed based on theoretical principles associated with shallow neural networks. According to the universal approximation theorem introduced by Hornik, Stinchcombe [2], a feedforward network with a single hidden layer is capable of approximating any continuous function, provided that a sufficient number of neurons and appropriate weights are used. Furthermore, Caudill [1] proposed that for a network with III input variables, an effective architecture may be obtained using approximately 2I+1 neurons in the hidden layer. Guided by these theoretical insights, ANN_2 is employed as a baseline model with a simpler structure, allowing for a systematic comparison between theory-based design and data-driven optimization approaches, particularly in the context of predicting responses at new and previously unseen locations.

*a) Model ANN_1*

To determine the optimal network configuration for ANN_1, a comprehensive hyperparameter optimization process was conducted using the Random Search method via the Keras Tuner framework. The search space was defined with a wide range to ensure global exploration, including the number of hidden layers (1 to 5), the number of neurons per layer (96 to 3104), dropout rate (0.0 to 0.5), and learning rate ($1\times10^{-4}$ to $5\times10^{-2}$).

The Rectified Linear Unit (ReLU) activation function was employed for hidden layers to facilitate non-linear feature extraction, while the hyperbolic tangent (tanh) function was utilized in the output layer for target normalization. The Adam optimizer was selected for its adaptive learning rate properties, supplemented by early stopping and learning rate reduction on plateau strategies to ensure stable convergence and prevent overfitting.

Training Convergence Behavior. The training and validation loss curves for the optimized ANN_1 model are illustrated in Figure 4. Both curves exhibit a sharp initial decline, followed by a steady, monotonic decrease toward low MSE values. The proximity and parallel trajectory of the two curves suggest a high degree of generalization. The dotted vertical line identifies the best epoch (approximately epoch 385), where the validation loss reached its minimum. The absence of significant divergence or oscillations confirms that the model achieved a stable balance between bias and variance.

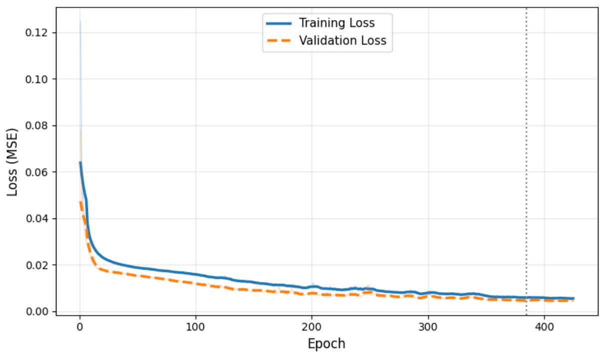


**Figure 4.** *Training and Validation loss vs Epoch (ANN_1)*

Influence of the Number of Hidden Layers. The impact of network depth on validation MSE is visualized using boxplots in Figure 5). The analysis shows that models with two and three hidden layers achieved the lowest median MSE and demonstrated high stability. Single-layer architectures and deeper configurations (4 to 5 layers) exhibited higher variance and, in several cases, significantly higher outlier errors (MSE > 0.2), indicating a higher risk of underfitting or unstable optimization. While a 2-layer setup appears to be a local optimum in this single-factor analysis, the global optimization process reveals that a three-layer configuration provides superior performance when integrated with specific unit counts and dropout rates.

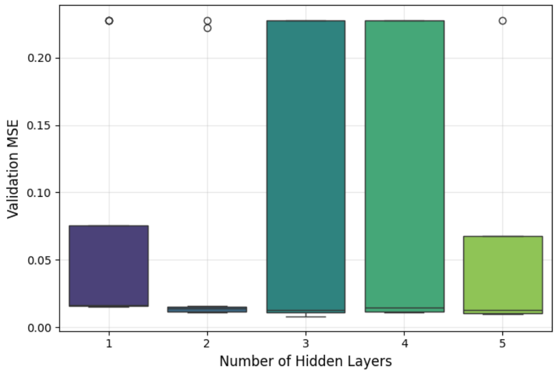


**Figure 5.** *Influence of the number of hidden layers on ANN_1 performance*

Influence of the Number of Hidden Units. Figure 6 displays the distribution of validation MSE relative to the total number of hidden units across all layers. The results indicate that the most accurate models are distributed within the range of 1000 to 3000 total units, as well as a cluster around 8000 units. This suggests that while moderate complexity is sufficient, the model can effectively utilize higher capacity if properly regularized. The heatmap in Figure 7 further refines this observation by focusing on the first hidden layer (Layer 0). The optimal performance zone is identified at 1824 units in the first layer combined with a low learning rate, achieving a minimum validation MSE of 0.00022.

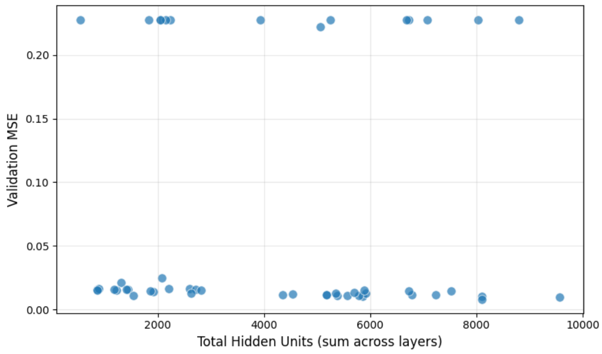


**Figure 6.** *Influence of total hidden units on ANN_1 performance*

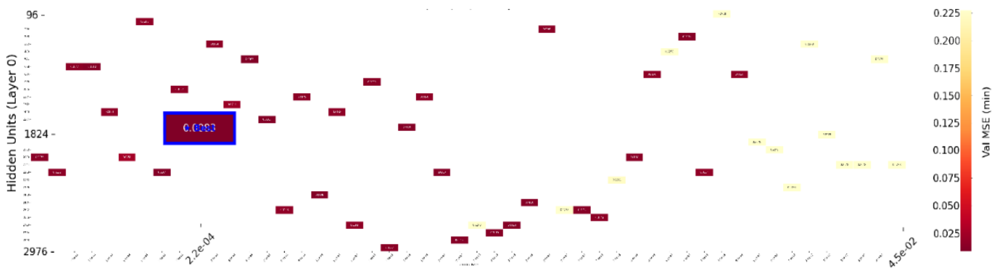


**Figure 7.** *Heatmap for Units (layer 0) vs Learning Rate vs MSE (ANN_1)*

Influence of the Learning Rate. The sensitivity of ANN_1 to the learning rate is analyzed in Figure 8. The scatter plot (Figure 8b) on a log scale reveals that stable and high-performing models are exclusively found within the narrow window of $1\times10^{-4}$ to $1\times10^{-3}$. Beyond a learning rate of $2\times10^{-3}$, the validation MSE increases dramatically to approximately 0.23, indicating a total failure of the convergence process. The grouped analysis in Figure 8a confirms that the optimal learning rate is $2.2\times10^{-4}$, which provides the best compromise between convergence speed and error minimization.

Interaction of Hyperparameters and Optimal Configuration. The findings highlight that the model's efficacy is a result of the complex interaction between depth, capacity, and regularization. Although the parametric study of layers (Figure 5) showed strong performance at two layers, the global search identified a 3-hidden-layer architecture as the final optimal solution. This underscores the necessity of multi-dimensional tuning to capture the non-linear dependencies between hyperparameters.

Based on the Keras Tuner results, the final optimal configuration for ANN_1 is summarized as follows: Number of Hidden Layers = 3; Neuron counts = [1824, 3168, 3104]; Dropout rates = [0.1, 0.2, 0.1]; Learning rate = $2.2\times10^{-4}$.

Given the relatively high capacity of ANN_1 (totaling 8,096 neurons across three hidden layers), several complementary regularization mechanisms were employed to prevent overfitting: (i) Dropout layers with rates of [0.1, 0.2, 0.1] were inserted between hidden layers to act as stochastic regularizers; (ii) a conservative learning rate of $2.2\times10^{-4}$ was selected through systematic hyperparameter search to ensure smooth convergence; (iii) Early Stopping was applied to terminate training when the validation loss ceased to improve (best epoch ≈ 385); and (iv) ReduceLROnPlateau was used to adaptively reduce the learning rate during plateaus. Collectively, these strategies constrain the effective model capacity and ensure that the network learns generalizable representations rather than memorizing training samples.

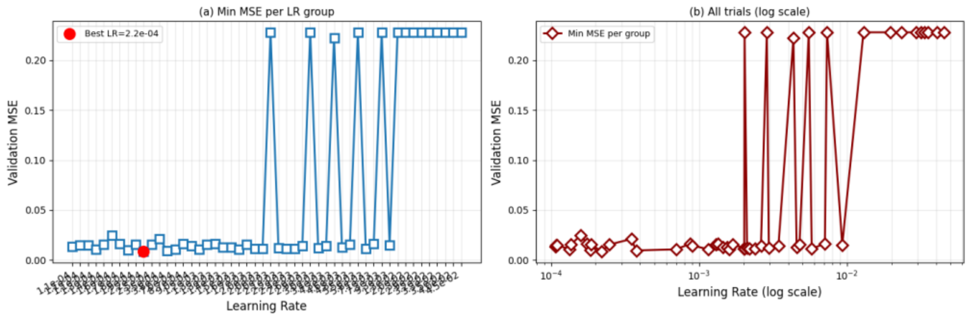


**Figure 8.** *Influence of the learning rate on ANN_1 performance [50 trials]*

*b) Model ANN_2*

In contrast to the data-driven optimization of ANN_1, the development of ANN_2 followed a more structured, theory-based approach, focusing on a single-hidden-layer architecture. To ensure a robust evaluation of this shallower network, a systematic parametric study was performed, varying the number of hidden nodes and the learning rate across a broad spectrum to identify the optimal configuration for damage detection.

Influence of the Number of Hidden Nodes. The sensitivity of ANN_2 to its hidden layer capacity was investigated by varying the number of neurons from 32 to 3072. As illustrated in Figure 9, the validation MSE exhibits a consistent downward trend as the number of nodes increases. A significant improvement in predictive accuracy is observed when transitioning from a very small number of nodes (32–64) to moderate counts (128–512), where the MSE drops from approximately 0.0263 to 0.0159. Beyond 1024 nodes, the error curve continues to decline but at a much lower rate, indicating a state of diminishing returns. The lowest validation error was achieved at the maximum surveyed capacity of 3072 nodes, suggesting that despite its shallow structure, ANN_2 benefits significantly from a high-dimensional feature mapping in the hidden layer.

Influence of the Learning Rate. The impact of the learning rate on the convergence of ANN_2 is presented in Figure 10. The model demonstrates high sensitivity to this parameter, with the MSE decreasing sharply as the learning rate increases from $1\times10^{-4}$ to $1\times10^{-2}$. A learning rate that is too conservative ($1\times10^{-4}$) resulted in a relatively high validation error (MSE ≈ 0.0389), likely due to incomplete convergence within the allotted epochs. The performance reached its peak at a learning rate of $1\times10^{-2}$, achieving the minimum error of 0.01458. However, a further increase to $5\times10^{-2}$ led to a slight rise in MSE (0.01622), signaling the onset of stochastic oscillations near the global minimum.

Heatmap Analysis and Interaction Effects. The joint influence of hidden nodes and learning rate is visualized in the heatmap in Figure 12. The analysis reveals a clear "optimal corridor" where high neuron counts are paired with moderate-to-high learning rates ($5\times10^{-3}$ to $1\times10^{-2}$). Notably, the heatmap identifies a catastrophic failure zone at the highest surveyed learning rate ($5\times10^{-2}$) for node counts above 192, where the MSE jumps to approximately 0.2278. This indicates that for larger networks, excessively high learning rates prevent the optimizer from finding a stable solution. The global best configuration for ANN_2 within this grid search was found at 2048 nodes with a learning rate of $1\times10^{-2}$, yielding an optimal MSE of 0.0149.

Training Convergence Behavior. The training and validation loss curves for the optimized ANN_2 model are shown in Figure 11. The model exhibits a very smooth and stable convergence path, with both training and validation losses decreasing rapidly within the first 50 epochs and stabilizing thereafter. The gap between the two curves is exceptionally narrow, and the validation loss remains remarkably smooth without the transient spikes observed in deeper models. This behavior suggests that the single-layer architecture of ANN_2, when properly configured with sufficient neurons and an optimal learning rate, provides a very stable and well-generalized predictive framework, reaching its best performance at approximately epoch 300.

Optimal Configuration Summary. Based on the parametric analysis and heatmap evaluation, the final architecture for ANN_2 was determined to be a single-hidden-layer network with 2048 hidden nodes. The model was trained using the Adam optimizer with a learning rate of $1\times10^{-2}$. This configuration allows ANN_2 to achieve a high degree of predictive accuracy while maintaining the simplicity and computational efficiency characteristic of shallow neural networks.

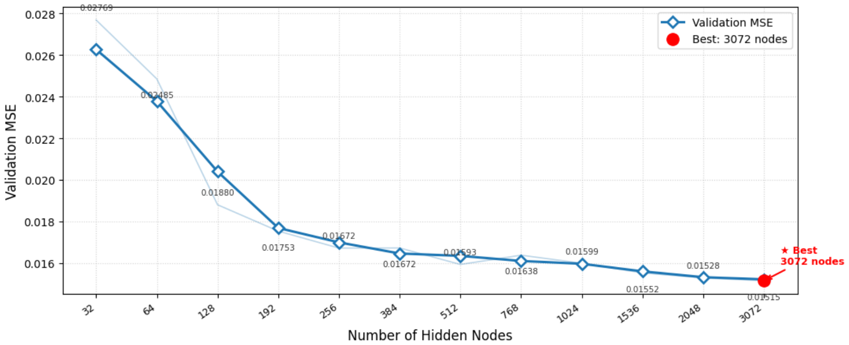


**Figure 9.** *Influence of the number of hidden units on ANN_2 performance*

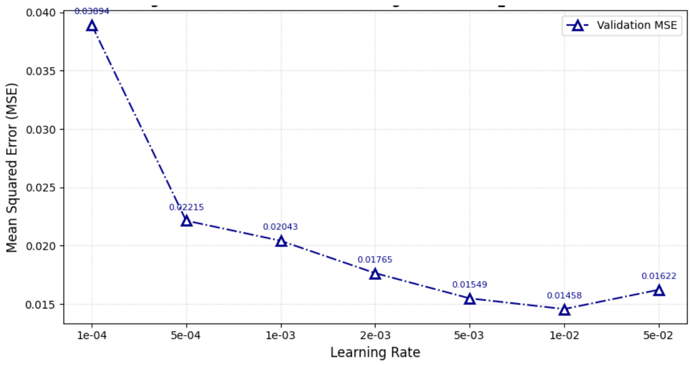


**Figure 10.** *Influence of the learning rate on ANN_2 performance*

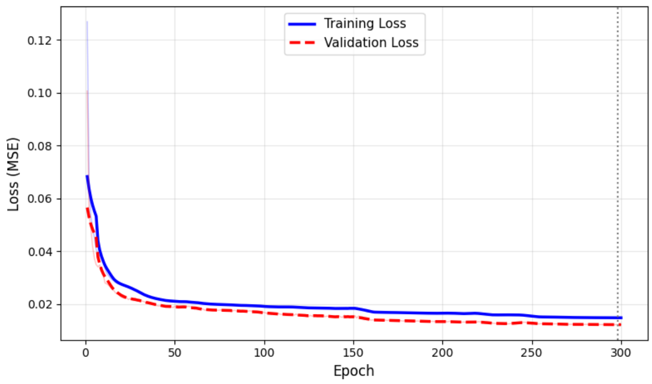


**Figure 11.** *Variation of Loss with Epoch (ANN_2)*

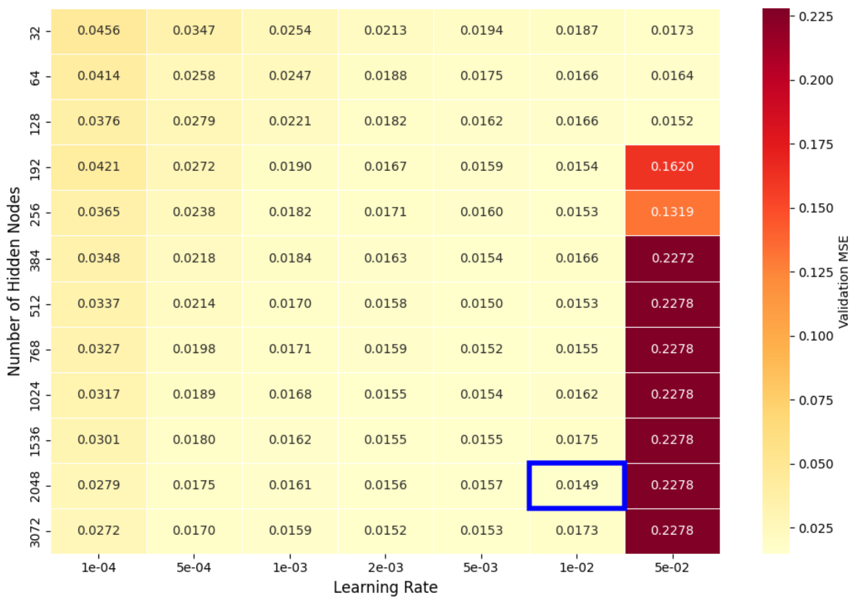


**Figure 12.** *Heatmap: Hidden Nodes vs Learning Rate vs MSE (ANN_2)*

### 4. Results and discussion

**Table 8.** *Statistical Metrics Performance for Training Data (train)*

| Model | Location_R² | Location_MSE | Width_R² | Width_MSE | Depth_R² | Depth_MSE |
|---|---|---|---|---|---|---|
| ANN 1 | 0.9970 | 244.1290 | 0.7755 | 0.1711 | 0.9155 | 0.2602 |
| ANN 2 | 0.9891 | 898.6354 | 0.2369 | 0.5818 | 0.8413 | 0.4883 |

**Table 9.** *Statistical Metrics Performance for Testing Data (test)*

| Model | Location_R² | Location_MSE | Width_R² | Width_MSE | Depth_R² | Depth_MSE |
|---|---|---|---|---|---|---|
| ANN 1 | 0.9889 | 914.0738 | 0.4729 | 1.0543 | 0.7019 | 2.3849 |
| ANN 2 | 0.9728 | 2240.4635 | 0.0650 | 1.8701 | 0.6067 | 3.1465 |

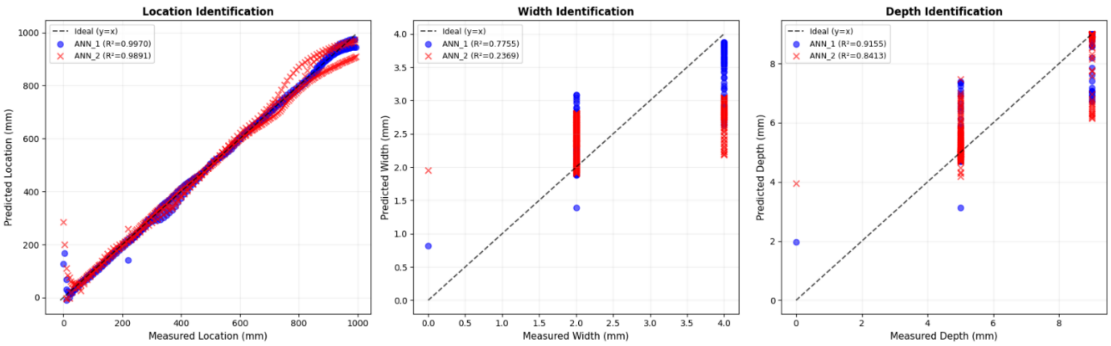


**Figure 13**. *Comparison of Predicted and Measured of two Model for Training Data*

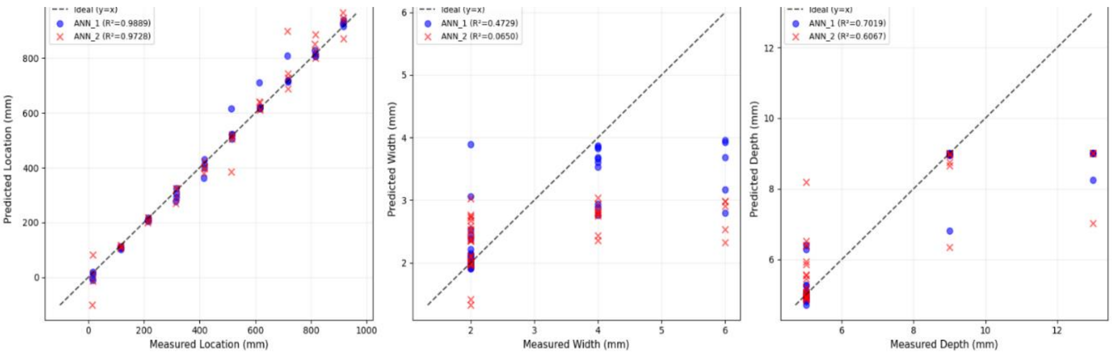


**Figure 14.** *Comparison of Predicted and Measured of two Model for Testing Data*

Prior to evaluating the predictive performance, it is important to verify that the trained models do not suffer from overfitting, particularly considering the high parameter count of ANN_1. Several diagnostic indicators confirm that overfitting did not occur. First, the loss curves shown in Figures 4 and 11 demonstrate smooth and monotonic convergence, with a narrow and stable gap between the training and validation losses throughout the training process. The absence of divergence between these curves indicates that the models learned generalizable patterns rather than memorizing the training data. Second, the train–test performance consistency further supports this conclusion. For the damage location target, ANN_1 achieved $R^2 = 0.9970$ on the training set and $R^2 = 0.9889$ on the test set, corresponding to a very small gap of only 0.0081, which indicates strong generalization capability. Although larger gaps were observed for width and depth, these differences are primarily due to the intentionally challenging out-of-distribution test samples rather than overfitting. Third, comparison with ANN_2, a shallow baseline network with substantially fewer parameters, provides additional evidence. ANN_2 consistently produced lower prediction accuracy on the test set across all three targets. If ANN_1 were overfitting, the lower-capacity ANN_2 would be expected to generalize better on unseen data; however, this behavior was not observed. Therefore, the superior performance of ANN_1 suggests that its additional network capacity improved representational learning instead of causing memorization. Overall, these findings demonstrate that the adopted regularization strategies, including Dropout, Early Stopping, and a conservative learning rate, were effective in controlling overfitting, and the reported test results reflect genuine generalization performance.

The predictive performance of the two ANN-based models was evaluated using statistical metrics and predicted–measured comparisons on both the training dataset (Table 8 and Figure 13) and a more challenging testing dataset (Table 9 and Figure 14). Notably, the test set consists of 40 scenarios, including entirely unseen damage locations and 10 cases where the width and depth exceed the range observed in the training data. This design introduces both spatial extrapolation and out-of-distribution (OOD) conditions, providing a rigorous assessment of model generalization.

Across all targets, ANN_1 consistently outperforms ANN_2, achieving higher $R^2$ and lower MSE in both training and testing phases. The performance gap becomes particularly evident under the challenging test conditions, confirming the superior robustness of ANN_1 when dealing with unseen and extrapolated scenarios.

Both models demonstrate strong capability in predicting damage location, even under unseen conditions. On the training set, ANN_1 achieves $R^2 = 0.9970$, slightly outperforming ANN_2 ($R^2=0.9891$). This trend remains consistent on the test set, where ANN_1 maintains $R^2=0.9889$, compared to $R^2=0.9728$ for ANN_2. The scatter plots (Figure 13 and Figure 14) show that predictions from both models align closely with the ideal line y=x, indicating that location is a relatively well-conditioned output. Importantly, even for entirely new spatial positions, both models retain high accuracy, suggesting that the relationship between natural frequencies and damage location is sufficiently smooth and learnable.

Although ANN_1 achieves slightly higher accuracy, its improvement in location prediction is relatively small ($\Delta R^2 \approx 0.0161$ on the test set) compared with its much higher computational cost. Therefore, when the main objective is only damage localization, ANN_2 may be a more practical choice because it provides good accuracy with lower computational demand. However, when the objective includes predicting damage geometry, such as width and depth, ANN_1 becomes more suitable due to its stronger learning capability and better performance under extrapolation conditions. These results suggest that ANN_2 is appropriate for efficient damage localization tasks, while ANN_1 is preferable for more detailed damage characterization in Structural Health Monitoring applications.

Width prediction presents a significantly more challenging task, especially under the test conditions where some samples exceed the training range. On the training data, ANN_1 achieves a moderate fit ($R^2=0.7755$), whereas ANN_2 performs poorly ($R^2=0.2369$). Under testing conditions, which include out-of-range width values, the performance of both models deteriorates, but the degradation is far more severe for ANN_2. Specifically, ANN_1 achieves $R^2=0.4729$, while ANN_2 drops sharply to $R^2=0.0650$, indicating near-random predictions. Figure 14 clearly shows that ANN_2 outputs are clustered and fail to follow the increasing trend, reflecting its inability to extrapolate beyond the training domain. In contrast, ANN_1 still captures partial trends, although with noticeable dispersion, highlighting its relatively better extrapolation capability.

A similar pattern is observed for depth prediction. On the training set, ANN_1 achieves $R^2=0.9155$, outperforming ANN_2 ($R^2=0.8413$). On the test set, which includes depth values beyond the training range, ANN_1 retains a reasonable predictive performance ($R^2=0.7019$), while ANN_2 drops to $R^2=0.6067$. The scatter plots indicate that ANN_2 predictions exhibit higher bias and reduced spread, particularly for larger depth values, suggesting difficulty in capturing nonlinear scaling behavior. ANN_1, although affected by extrapolation, maintains a closer alignment with the ideal trend, demonstrating stronger generalization.

The inclusion of new spatial locations and out-of-range width and depth values in the test set significantly increases the difficulty of the prediction task. These conditions require the models not only to interpolate within the learned domain but also to extrapolate beyond it. The results clearly indicate that ANN_1 is more robust to both spatial and parametric extrapolation, whereas ANN_2, due to its limited representational capacity, struggles to generalize under such conditions. The performance degradation observed in ANN_2, particularly for width, highlights its sensitivity to distribution shifts.

In summary, ANN_1 demonstrates superior performance across all targets and maintains greater robustness under challenging testing conditions involving unseen locations and out-of-distribution values. While ANN_2 performs adequately for simpler tasks such as location identification, it exhibits significant limitations in capturing complex nonlinear relationships required for accurate width and depth prediction. Notably, both ANN_1 and ANN_2 achieve comparable accuracy in predicting damage location; however, ANN_1 consistently outperforms ANN_2 in estimating crack width and depth. This suggests that for tasks limited to location identification, a shallow neural network may still provide sufficient accuracy. These findings confirm that the data-driven, optimally tuned ANN_1 model is more suitable for reliable multi-parameter damage characterization, especially in scenarios involving extrapolation beyond the training dataset.

## 5. Feature Importance Analysis using Permutation Method

To gain deeper insights into the contribution of each natural frequency to the prediction of damage characteristics, a Permutation Importance analysis was conducted on the ANN_1 model using the testing dataset. This method evaluates the importance of an input feature by measuring the increase in the model's prediction error (Mean Squared Error - MSE) and the decrease in the coefficient of determination (R2) after the feature's values are randomly shuffled. A larger change in these metrics indicates that the model relies more heavily on that specific feature for its predictions.

The analysis reveals that the first natural frequency (F1 ) is the most critical feature for identifying the damage location. As shown in the bar chart and heatmap of ΔMSE (Figure 15, Figure 16), permuting F1 leads to a massive surge in error, with an average increase of approximately $1.386\times10^5$. Correspondingly, the R2 value drops by 1.6799 (Figure 17), which is the most significant reduction among all input-output pairs. The second and third frequencies (F2 and F3) also contribute to location identification, with ΔMSE values of 25759 and 17844 (Figure 15), respectively. However, their impact is substantially lower than that of F1, suggesting that the fundamental mode of vibration carries the primary information regarding the spatial position of damage in the steel beam.

The sensitivity of width and depth predictions to the input frequencies follows a different pattern and exhibits lower absolute error magnitudes compared to location. For damage width, F1 remains the most influential parameter (ranking 1st), followed by F2 and F3. Shuffling F1 results in a $\Delta R^2$ of −1.0806 (Figure 17), confirming its dominant role even for complex geometrical characterization. In contrast, for damage depth identification, the second natural frequency (F2) emerges as the most important feature, followed by F3, while F1 ranks third. The permutation of F2 causes the highest error increase ΔMSE=6.502 (Figure 16) and the largest performance drop $\Delta R^2=-0.8127$ (Figure 17). This shift indicates that higher-order vibration modes are more sensitive to the reduction in cross-sectional stiffness caused by damage depth than the fundamental mode.

The hierarchical ranking of the frequencies for each target is summarized in the importance table. For both Location and Width, the order of importance is consistently F1>F2>F3. However, for Depth, the hierarchy shifts to F2>F3>F1.

These findings provide significant physical insights into the damage detection problem: while the first mode (F1) is highly sensitive to the spatial distribution and extent of damage, the second mode (F2) plays a vital role in characterizing the severity of the damage (depth). The results justify the inclusion of multiple natural frequencies as input features, as each mode provides complementary information necessary for the comprehensive identification of damage position, width, and depth in structural components.

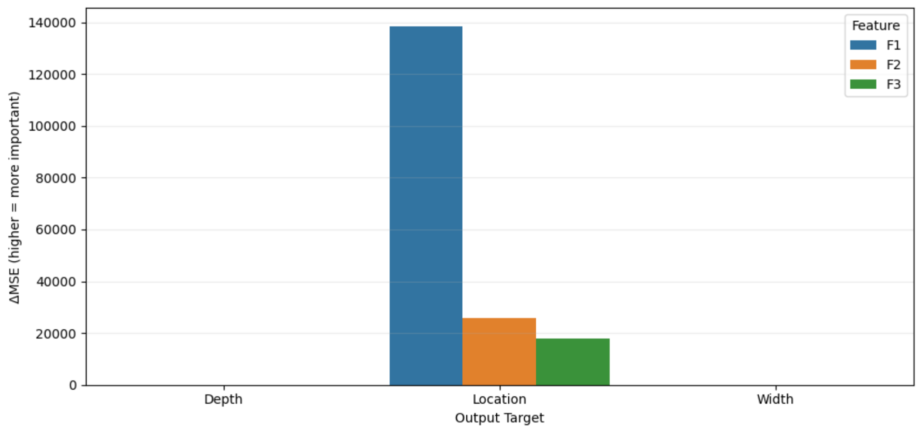


**Figure 15.** *Permutation importance (ANN_1, Test): ΔMSE when permuting each input feature*

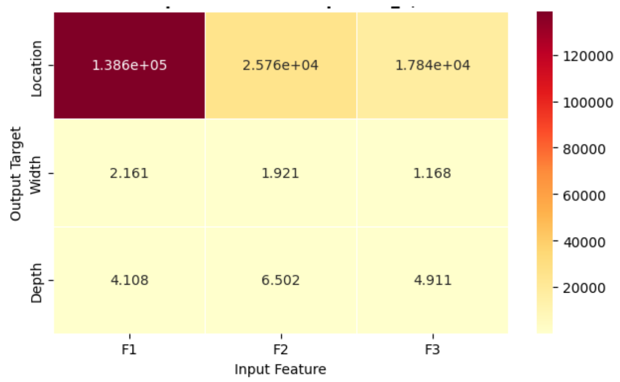


**Figure 16.** *Permutation importance heatmap (ANN_1, Test): ΔMSE*

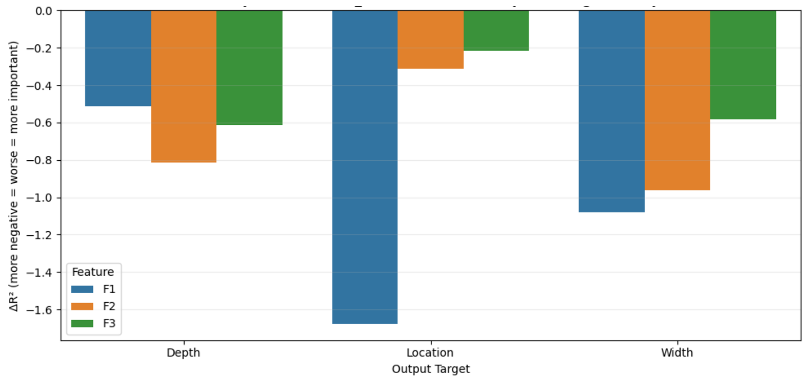


**Figure 17.** *Permutation importance (ANN_1, Test): ΔR2 when permuting each input feature*

## 6. Conclusions

By integrating experimental modal analysis (RFP), numerical simulation (FEM), and Artificial Neural Networks (ANN), this study developed a robust framework for the multi-parameter characterization of damage in steel beams. The investigation focused on predicting damage location, width, and depth using natural frequencies as input features. The key findings of this research are as follows:

– The FEM-RFP framework provides a reliable foundation for generating representative synthetic datasets for vibration-based damage identification, especially when experimental data are limited;

– Both ANN_1 and ANN_2 predict damage location with high accuracy ($R^2 > 0.97$) on the testing set), indicating that natural frequencies capture location information effectively even for unseen positions;

– For location-only applications, the shallow ANN_2 model remains a practical and sufficient solution because of its lower complexity, stable convergence, and easier deployment on resource-constrained monitoring platforms;

– The estimation of width and depth is more challenging than location prediction, mainly because these parameters are more sensitive to extrapolation and distribution shifts;

– For such multi-parameter tasks, ANN_1 offers more robust and consistent performance than ANN_2, particularly under unseen and out-of-distribution damage conditions;

– The results support a tiered SHM strategy, in which ANN_2 is suitable for continuous low-cost localization, while ANN_1 is better suited for detailed geometric characterization when higher model capacity is required.

Although the proposed ANN-based methodology showed promising performance for vibration-based damage identification, several limitations remain. This study considered only single-damage cases and simplified stiffness reduction, whereas real structures may involve multiple damages and combined failure mechanisms. Future work will extend the framework to multi-damage detection using richer FEM datasets, additional modal features, and advanced deep learning models such as CNNs and GNNs. Although the FEM model was validated experimentally, large-scale field validation is still needed. Future studies will also incorporate uncertainty quantification methods, including Bayesian Neural Networks and Monte Carlo Dropout, to improve robustness under noise and environmental variability in practical SHM applications.

**REFERENCES**


[1] Caudill Maureen (1988). *"Neural networks primer, Part III".* AI Expert, 3 (6), pp 53-59.

[2] Hornik Kurt, Stinchcombe Maxwell, and White Halbert (1989). *"Multilayer feedforward networks are universal approximators".* Neural networks, 2 (5), pp 359-366.

[3] Maier HR and Dandy GC (2000), *Application of artificial neural networks to forecasting of surface water quality variables: issues, applications and challenges*, in Artificial neural networks in hydrology. Springer. p. 287-309.

[4] Shahin Mohamed A (2010). *"Intelligent computing for modeling axial capacity of pile foundations".* Canadian Geotechnical Journal, 47 (2), pp 230-243.

[5] Cuong-Le Thanh, et al. (2021). *"An efficient approach for damage identification based on improved machine learning using PSO-SVM".* Engineering with Computers, pp 1-16.

[6] Ghadimi Siamak and Kourehli Seyed Sina (2017). *"Crack detection of structures using modified extreme learning machine (MELM)".* Inverse Problems in Science and Engineering, 25 (7), pp 995-1013.

[7] Gillich Gilbert-Rainer, et al. (2019). *"A robust damage detection method based on multi-modal analysis in variable temperature conditions".* Mechanical Systems and Signal Processing, 115 pp 361-379.

[8] Gillich Gilbert-Rainer, et al. (2016). *"Free vibration of a perfectly clamped-free beam with stepwise eccentric distributed masses".* Shock and Vibration.

[9] Gillich Nicoleta, et al. (2022). *"Beam damage assessment using natural frequency shift and machine learning".* Sensors, 22 (3), pp 1118.

[10] Khatir Samir, et al. (2020). *"An efficient hybrid TLBO-PSO-ANN for fast damage identification in steel beam structures using IGA".* Smart Structures and Systems, 25 (5), pp 605-617.

[11] Khatir Samir and Wahab Magd Abdel (2019). *"A computational approach for crack identification in plate structures using XFEM, XIGA, PSO and Jaya algorithm".* Theoretical and Applied Fracture Mechanics, 103 pp 102240.

[12] Lee Jong-Won, Kim Sang-Ryul, and Huh Young-Cheol (2014). *"Pipe crack identification based on the energy method and committee of neural networks".* International Journal of Steel Structures, 14 (2), pp 345-354.

[13] Mortazavi SNS and Ince A (2020). *"An artificial neural network modeling approach for short and long fatigue crack propagation".* Computational Materials Science, 185 pp 109962.

[14] Richardson Mark H and Formenti David L (1982). "*Parameter estimation from frequency response measurements using rational fraction polynomials"*. in Proceedings of the 1st international modal analysis conference. Union College Schenectady, NY.

[15] Rumelhart David E, Hinton Geoffrey E, and Williams Ronald J (1985), Learning internal representations by error propagation, Institute for Cognitive Science, University of California, San Diego La...

[16] Samir K, et al. (2015). "*Genetic algorithm based objective functions comparative study for damage detection and localization in beam structures"*. in Journal of Physics: Conference Series. IOP Publishing.

[17] Seguini Meriem, et al. (2022). *"Crack prediction in beam-like structure using ANN based on frequency analysis".* Frattura ed Integrità Strutturale, 16 (59), pp 18-34.

[18] Seguini Meriem, et al. (2021). *"Crack prediction in pipeline using ANN-PSO based on numerical and experimental modal analysis".* Smart Structures and Systems, 27 (3), pp 507-523.

[19] Swamidas ASJ, Yang Xia, and Seshadri R (2004). *"Identification of cracking in beam structures using Timoshenko and Euler formulations".* Journal of Engineering Mechanics, 130 (11), pp 1297-1308.

[20] Vu Van Tuan, et al. (2025). *"Damage detection in steel beams using natural frequency analysis and machine learning techniques".* The Journal of Strain Analysis for Engineering Design, pp 03093247251327622.

[21] Vu Van Tuan, Thom Do Van, and Tran Trung Duc (2024). *"Identification of damage in steel beam by natural frequency using machine learning algorithms".* Proceedings of the Institution of Mechanical Engineers, Part C: Journal of Mechanical Engineering Science, 238 (19), pp 9644-9659.

[22] Yang XF, Swamidas ASJ, and Seshadri R (2001). *"Crack identification in vibrating beams using the energy method".* Journal of sound and vibration, 244 (2), pp 339-357.

[23] Zhou Yun-Lai, Maia Nuno MM, and Abdel Wahab Magd (2018). *"Damage detection using transmissibility compressed by principal component analysis enhanced with distance measure".* Journal of Vibration and Control, 24 (10), pp 2001-2019.

[24] Zhou Yun-Lai, et al. (2017). *"Structural damage detection using transmissibility together with hierarchical clustering analysis and similarity measure".* Structural health monitoring, 16 (6), pp 711-731.